Phase synchronization of baroclinic waves in a differentially heated rotating annulus experiment subject to periodic forcing with a variable duty cycle

P. L. Read, X. Morice-Atkinson, E. J. Allen, and A. A. Castrejón-Pita

Citation: Chaos **27**, 127001 (2017); doi: 10.1063/1.5001817
View online: http://dx.doi.org/10.1063/1.5001817
View Table of Contents: http://aip.scitation.org/toc/cha/27/12
Published by the American Institute of Physics

Phase synchronization of baroclinic waves in a differentially heated rotating annulus experiment subject to periodic forcing with a variable duty cycle

P. L. Read,[1,a)] X. Morice-Atkinson,[1,b)] E. J. Allen,[1,2,c)] and A. A. Castrejón-Pita[3]
[1]*Department of Physics, University of Oxford, Oxford, United Kingdom*
[2]*Department of Physics, University of Manchester, Manchester, United Kingdom*
[3]*Department of Engineering Science, University of Oxford, Oxford, United Kingdom*

(Received 16 January 2017; accepted 31 March 2017; published online 18 September 2017)

A series of laboratory experiments in a thermally driven, rotating fluid annulus are presented that investigate the onset and characteristics of phase synchronization and frequency entrainment between the intrinsic, chaotic, oscillatory amplitude modulation of travelling baroclinic waves and a periodic modulation of the (axisymmetric) thermal boundary conditions, subject to time-dependent coupling. The time-dependence is in the form of a prescribed duty cycle in which the periodic forcing of the boundary conditions is applied for only a fraction δ of each oscillation. For the rest of the oscillation, the boundary conditions are held fixed. Two profiles of forcing were investigated that capture different parts of the sinusoidal variation and δ was varied over the range $0.1 \leq \delta \leq 1$. Reducing δ was found to act in a similar way to a reduction in a constant coupling coefficient in reducing the width of the interval in forcing frequency or period over which complete synchronization was observed (the "Arnol'd tongue") with respect to the detuning, although for the strongest pulse-like forcing profile some degree of synchronization was discernible even at $\delta = 0.1$. Complete phase synchronization was obtained within the Arnol'd tongue itself, although the strength of the amplitude modulation of the baroclinic wave was not significantly affected. These experiments demonstrate a possible mechanism for intraseasonal and/or interannual "teleconnections" within the climate system of the Earth and other planets that does not rely on Rossby wave propagation across the planet along great circles. [http://dx.doi.org/10.1063/1.5001817]

Synchronization is commonly discussed in the context of discrete, coupled oscillators which may be periodic or chaotic. But under some circumstances, extended nonlinear systems which are formally infinite-dimensional, such as fluid flows, may exhibit discrete oscillations and behave as if they consisted of discrete oscillating components. We study such an example in the laboratory, consisting of amplitude-modulated, azimuthally travelling baroclinic waves in a thermally driven, rotating annulus experiment. Earlier experiments showed that, under conditions in which the unperturbed travelling waves are spontaneously (either periodically or weakly chaotically) modulated in time, the amplitude modulation of the waves can be phase-locked and synchronized with periodic perturbations of the applied (axisymmetric) temperature difference between the inner and outer cylinders of the experiment. We use this potentially synchronized system to explore what happens if the periodic perturbations are applied for only a given fraction of each cycle—i.e., for a duty cycle <100%. Our systematic exploration of variations in both the duty cycle and detuning (difference in period between the natural oscillation period and that of the imposed boundary temperature variations) shows that the duty cycle acts in the same way as a variable coupling coefficient, demonstrating a narrowing of the frequency interval over which complete phase synchronization is observed as the duty cycle is reduced. We also report a new form of scaling of residual phase fluctuations within the synchronized state with the duty cycle parameter, which may apply more generally with respect to coupling coefficients. These results are relevant, among other things, to our understanding of possible mechanisms coupling different components of the climate system of Earth and other planets, and their impact leading to potentially correlated behaviour in different parts of the world during different seasons, even if the coupling between these regions is not present throughout the year.

I. INTRODUCTION

Synchronization is generally taken to imply a correlated behavior between two or more oscillating systems, in which the oscillations of one system follow that of another. It takes a number of forms depending on the degree of coherence between the systems, ranging from complete synchronization (where every feature of the behavior of the systems behaves

[a)]Atmospheric, Oceanic and Planetary Physics, Clarendon Laboratory, Parks Road, Oxford OX1 3PU, United Kingdom. Electronic mail: peter.read@physics.ox.ac.uk
[b)]Now at Institute of Cosmology and Gravitation, University of Portsmouth, Portsmouth, United Kingdom.
[c)]Now at Quantum Engineering Technology Labs and the Quantum Engineering Centre for Doctoral Training, H. H. Wills Physics Laboratory and Department of Electrical and Electronic Engineering, University of Bristol, Bristol, United Kingdom.

coherently) through weaker forms, such as phase synchronization [which is the form most commonly discussed, e.g., Rosenblum *et al.* (1996) and Pikovsky *et al.* (2001)], partial synchronization, and the so-called generalized synchronization (Rulkov *et al.* 1995). The essential elements required for synchronization typically include some form of coupling between components of the oscillating systems which can exert an influence on the phase of the oscillations, enabling the frequency of one system to be entrained by another into a constant ratio (on average), typically of simple integers. Such systems have been widely studied for many years with diverse applications in both discrete and continuum systems, such as in networks of physical or biological systems (e.g., Watts and Strogatz, 1998 and Arenas *et al.*, 2008), ensembles of chemical oscillators (e.g., Taylor *et al.*, 2009), lasers (e.g., Van Wiggeren and Roy 1998), cardiac and circadian rhythms (Glass 2001), reaction-diffusion systems, and in mechanically oscillating systems among many others (e.g., see Pikovsky *et al.*, 2001).

Although initially restricted to systems of simple, periodic oscillators, the concept of synchronization is now also widely applied in the context of chaotic oscillators, in which spontaneously aperiodic behavior can also be entrained to follow an external signal or the behavior of another component of the network under some circumstances (e.g., Pecora *et al.*, 1997 and Boccalletti *et al.*, 2002). This has broadened the application of synchronization concepts much more widely to problems in engineering, cryptography, biology, medicine, and physics [such as in nonlinear optics—e.g., see Van Wiggeren and Roy (1998)]—see e.g., Bocalletti *et al.* (2002) for a review. Most applications, however, have generally focused on systems of discrete oscillators (periodic or chaotic) though potentially in very large and complex interconnected networks (Watts and Strogatz, 1998 and Arenas *et al.*, 2008). But continuous (formally infinite dimensional) systems, such as fluids or plasmas, can also behave as if they consist of a finite (countable) set of discrete component oscillators under certain circumstances, given appropriate forcing and dissipation (e.g., Williamson and Govardhan, 2004; Pereira *et al.*, 2013; and Goldstein *et al.*, 2016), especially for flows confined within finite-sized containers. This raises the possibility of observing discrete, synchronized behavior within fluid dynamical systems that may be analogous to synchronization phenomena in networks of discrete oscillators.

Such behavior has been explored in the context of theoretical and numerical models, laboratory experiments, and even in observations of large-scale natural systems such as the Earth's atmosphere and climate system, which Lorenz (1991) suggested could be regarded as a complex network of weakly coupled (regional) sub-systems. Early explorations of synchronization phenomena in meteorology and climate were prompted by an interest in accounting for the so-called "teleconnections" in the atmosphere, in which geographically widely separated events may be causally related by various coupling mechanisms. Mechanistic studies of these phenomena were initially based on discretized (often highly truncated) numerical models of atmospheric flows in distinct regions of the atmosphere (mid-latitude channels or whole hemispheres) in which *ad hoc* coupling of all (or most) flow components between models was imposed (e.g., Duane, 1997 and Lunkheit, 2001). Later work, however, showed that only weak coupling of a subset of flow components (usually non-zonal eddies) was needed to achieve discernible synchronization (e.g., Kocarev *et al.*, 1997; Duane *et al.*, 1999; Duane and Tribbia, 2001; 2004; and Hiemstra *et al.*, 2012). In a precursor to the present work, Duane *et al.* (1999) also conducted some simulations in which the cross-hemispheric Rossby wave coupling they invoked to account for synchronized atmospheric blocking events between the north and south varied with the time of year, although this was not investigated in much detail.

Meteorological data assimilation, in which observations are introduced into a numerical simulation of the atmosphere or oceans, has also been reinterpreted in terms of the synchronization of chaotic systems through weak coupling of a subset of simulated flow components with sequences of observations (e.g., Duane *et al.*, 2006; Yang *et al.*, 2006; and Abarbanel *et al.*, 2009). This approach has been further developed most recently in the context of multi-model ensembles of climate simulations as a means of accounting for systematic errors between different models through mutual assimilation of model variables, forming the so-called "super-model" (van den Berge *et al.*, 2011; Duane, 2015; and Shen *et al.*, 2016).

Evidence for actual identifiable synchronization phenomena within the Earth's climate system has also been sought through analysis of the time series of climate observations [e.g., see Read and Castrejón-Pita (2010) for a review]. Duane *et al.* (1999), for example, noted a weak tendency for blocking events to occur simultaneously in both the northern and southern hemispheres under certain conditions/at certain times of the year. Maraun and Kurths (2005) found evidence for phase synchronization between the El Niño-Southern Oscillation (ENSO) index and variations in the Indian Monsoon, while Feliks *et al.* (2010) detected phase synchronization between various climate indicators in the middle East and the North Atlantic Oscillation (Hurrell *et al.*, 2003) on timescales of 7–8 years. On annual/seasonal timescales, Gruzdev and Bezverkhny (2000), Kuai *et al.* (2009), and Read and Castrejón-Pita (2012), showed that the stratospheric Quasi-Biennial Oscillation (QBO) was phase-synchronized with the annual cycle in that its period was found to be entrained to a rational ratio of the annual period, although this ratio evidently fluctuated chaotically on timescales of several years. Evidence of partial phase synchronization of the ENSO index to the annual cycle was also found by Stein *et al.* (2011).

Concerning laboratory fluid flow experiments, Maza *et al.* (2000), for example, demonstrated synchronization phenomena within a chaotic convective flow in a rectangular box to which oscillatory thermal perturbations were applied locally to a small region of the upper surface. Maestrello (2004) studied synchronized interactions between a turbulent aerodynamic boundary layer and an adjacent flexible boundary and other sustained resonant interactions between mechanical structures and periodic vortex shedding were

reviewed by Williamson and Govardhan (2004). Most relevant to the present study, Eccles *et al.* (2009) investigated synchronization effects in a rotating, thermally driven annulus experiment in which the basic (unperturbed) flow consisted of a rotating, temporally modulated travelling baroclinic wave that propagated azimuthally around the annular channel. Clear synchronization was observed between oscillations of the wave amplitude and cyclic perturbations of the imposed (axisymmetric) temperature contrast, provided the period of the perturbations was not too far removed from that of the natural period of the wave amplitude modulation. Phase synchronization with the periodically perturbed thermal boundary conditions was observed in both quasi-periodic and chaotic regimes. This was taken one stage further by Castrejón-Pita and Read (2010), who coupled two such experimental chambers via their (azimuthally symmetric) boundary conditions in a master-slave configuration, such that fluctuations in the heat transport in one annulus could influence the boundary conditions of the other. They were able to demonstrate phase synchronization of the wave modulation in the slave system in both quasi-periodic and chaotic regimes.

In the present work, we extend the experiments of Eccles *et al.* (2009) and Castrejón-Pita and Read (2010) to explore the impact of *time-dependent* coupling on the tendency of the baroclinic wave system to synchronize with periodic modulations in the thermal boundary conditions, by imposing a duty cycle on the applied perturbations. In many respects, this forms a laboratory analogue of the hemispheric coupling model simulations of Duane *et al.* (1999), with the important difference that, in our experiments, the coupling between the applied perturbation and the experimental flow is imposed axisymmetrically, via the "annular mode" in the parlance of climate dynamics. One possible motivation was to explore the potential for such annular mode coupling (essentially via modulations in the effective hemispheric heat transfer) to result in significant cross-hemispheric synchronization, even if the coupling is only effective during certain seasons of the year. Such a configuration may be seen as the prototype of a whole new class of "climate teleconnections" which does not rely on Rossby wave propagation from one region to another (cf. Hoskins and Karoly 1981).

Section II describes the experimental configuration, introducing the key variables to be explored and the methods of analysis. The main results are presented in Sec. III and the overall conclusions are discussed in Sec. IV.

II. EXPERIMENTAL CONFIGURATION

The apparatus was modified from the thermally driven, rotating annulus experiment used in earlier studies by Hignett *et al.* (1985), Read *et al.* (1992), Früh and Read (1997), Read (2003), Eccles *et al.* (2009), and Castrejon-Pita *et al.* (2010). It comprised two upright, coaxial brass cylinders, mounted along the rotation axis of a horizontal rotating table with flat, thermally insulating (Perspex) horizontal boundaries, both of which were in contact with the working fluid in the annular channel. Water was circulated in two separate, independently controlled channels at two well-controlled temperatures in thermal contact with each sidewall to maintain quasi-isothermal boundaries. The temperature of the water in each circuit was maintained to a precision of ± 0.01 K by a combination of inline chillers, heaters, and platinum resistance thermal sensors, servo-controlled by a commercial process controller (*Eurotherm 2704*). Pumps and chillers were located in the stationary laboratory frame and the coolant was circulated onto and off of the rotating frame via rotating fluid couplers. The whole apparatus in the rotating frame was placed inside a temperature controlled enclosure, whose air temperature was maintained at ± 0.5 K by a thermostatically controlled heater, within the laboratory whose temperature was maintained at around ± 1.5 K. The dimensions and parameters for the experiments described herein are listed in Table I, and a schematic diagram and photograph of the apparatus are depicted in Fig. 1.

In common with other studies using rotating annulus experiments (e.g., see Hide and Mason, 1975 and Read *et al.*, 2015), the parameter space is determined with reference to two principal dimensionless parameters, the thermal Rossby or Hide number defined as

$$\Theta = \frac{g\alpha \Delta T d}{\Omega^2 (b-a)^2}, \tag{1}$$

where g is the acceleration due to gravity and other parameters are shown in Table I, and a form of Taylor number scaled by the aspect ratio,

$$\Im = \frac{4\Omega^2 (b-a)^5}{\nu^2 d} = \frac{4\Omega^2 \mathrm{L}^4}{\nu^2} \frac{L}{d}, \tag{2}$$

TABLE I. Annulus properties.

	Symbol	Value	Precision	Unit
Vol. of convection chamber	…	2.54	…	L
Depth	d	140.0	± 0.2	mm
Inner radius	a	25.0	± 0.1	mm
Outer radius	b	80.0	± 0.1	mm
Rotation rate	Ω	1.6	$\pm 3 \times 10^{-5}$	rad s^{-1}
Outer circuit temperature	T_b	23.31	± 0.01	°C
Inner circuit temperature	T_a	15.00	± 0.01	°C
Temperature difference	$\Delta T = T_b - T_a$	8.31	± 0.02	°C
Density	ρ	1.081×10^3	± 0.001	kg m^{-3}
Glycerol fraction by vol.	…	0.26575	…	…
Glycerol fraction by mass	…	0.31423	…	…
Kinematic viscosity[1]	ν	2.3243×10^{-6}	…	m^2 s^{-1}
Thermal expansion coefficient[2]	α	3.69×10^{-4}	…	K^{-1}
Thermal Rossby number	Θ	0.544	± 0.05	
Taylor number	$\Im$	6.82×10^6	$\pm 1.0 \times 10^5$	

[1]Kinematic viscosity was determined following Cheng (2008)
[2]Thermal Expansion Coefficient was determined following Cristancho *et al.* (2011)

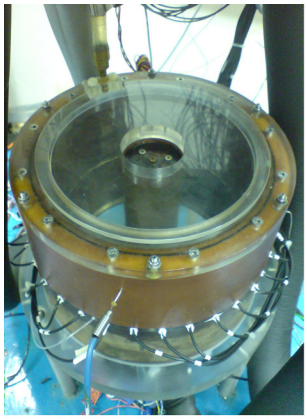

(a)

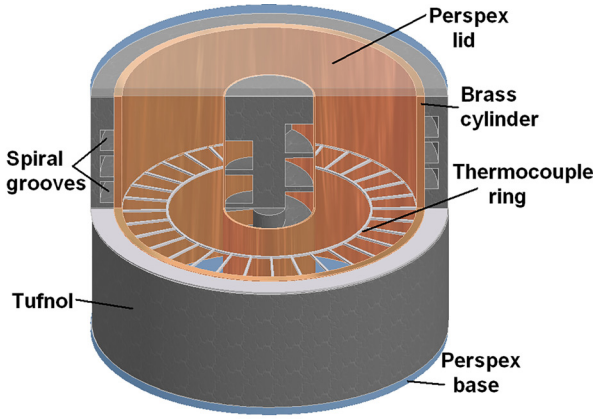

(b)

FIG. 1. (a) Photograph of experimental apparatus showing the annular convection chamber on the rotating table. (b) Schematic of the rotating annulus showing inner and outer cylinders and the circular array of thermocouples at mid-height and mid-radius. The working fluid is contained within the annular channel between the cylinders. The outer cylinder is heated from the outside, and the inner cylinder is cooled from the inside. Ω is the rotation rate, and $\Delta T = |T_a - T_b|$ is the applied temperature difference.

where $L = (b - a)$ is the radial width of the channel, following the study by Fowlis and Hide (1965). The measurement system for the annulus involved acquiring data from copper-constantan thermocouples in a ring with 32 equally spaced sensors in the azimuthal plane, positioned at mid-height and mid-radius, together with additional thermocouple sensors embedded in the sidewall boundaries and others to sample the ambient air temperature. These temperature measurements were digitized by an on-board Agilent 30904A Data Acquisition system in the rotating frame at a sample interval of 4 s, and sent in real time to a computer (in the stationary laboratory frame, connected via electrical slip rings) for further analysis. The rotation of the table was maintained to a precision of a few parts in 10^5 through analogue servo-control of the DC direct-drive motor via a tachometer.

A. Coupling and synchronization

As employed by Castrejón-Pita *et al.* (2010), cyclic, controlled perturbations to the sidewall boundary temperatures were applied through an additional in-line heater, placed after the Eurotherm control sensor, whose heating rate was controlled in real time by the computer in the stationary laboratory frame. The applied boundary temperature was then monitored by thermistor probes. In the cases investigated by Eccles *et al.* (2009), the perturbations applied to the thermal boundary conditions consisted of periodic (sinusoidal) variations in T_a and T_b such that $\Delta T = \Delta T_0 + \epsilon \sin \gamma t$. The amplitude of the forcing, ϵ, was kept fixed and the frequency, γ, was chosen to be close to that of the natural vacillation frequency of the baroclinic wave flow.

For the purposes of this experiment, the effect of intermittent coupling was achieved by switching off the periodic forcing for a certain fraction of each cycle (i.e., imposing a *duty cycle* δ) to vary the degree of forcing. This was achieved using one of two different methods, as illustrated in Figs. 2 and 3. Upon imposing a duty cycle on the periodic forcing using profile 1, the forcing closely followed the sinusoidal oscillation in ΔT for times centred around the peak or trough of each oscillation, deviating back to the nominal reference value around the time of the zero-crossing. When imposing a duty cycle on the periodic forcing using profile 2, however, the forcing was applied only for part of the positive-going phase of each cycle, thereby acting more like a pulse to try to "kick" the system back into synchronization during each period.

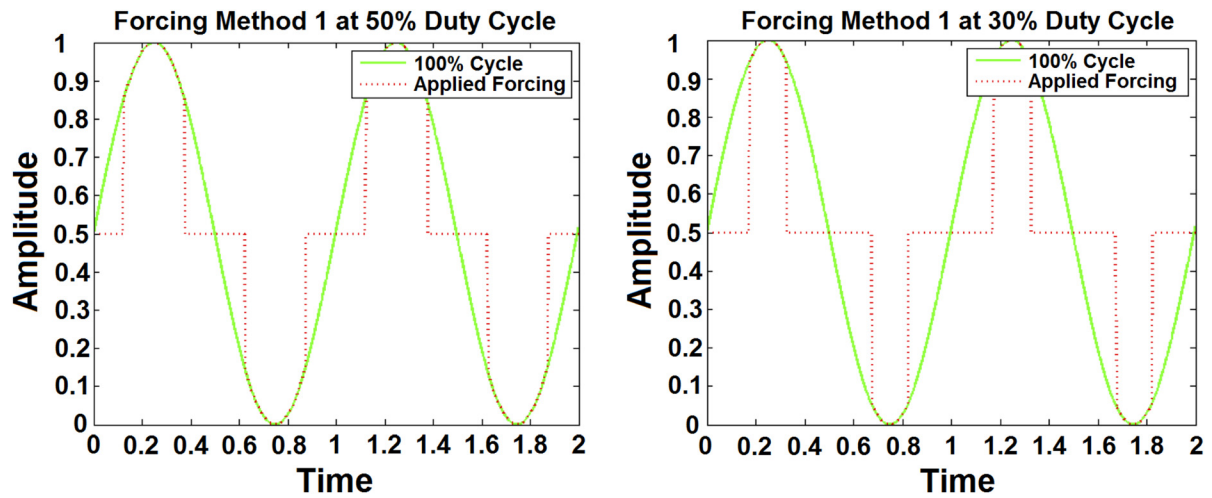

FIG. 2. Forcing profile 1 at duty cycle $\delta = 50\%$ (left) and $\delta = 30\%$ (right). This figure shows the applied forcing (dotted red line) following the imposed sinusoidal form (solid green line), with horizontal line segments indicating time intervals when the temperature is held constant—the duty cycle is modified by varying this time interval.

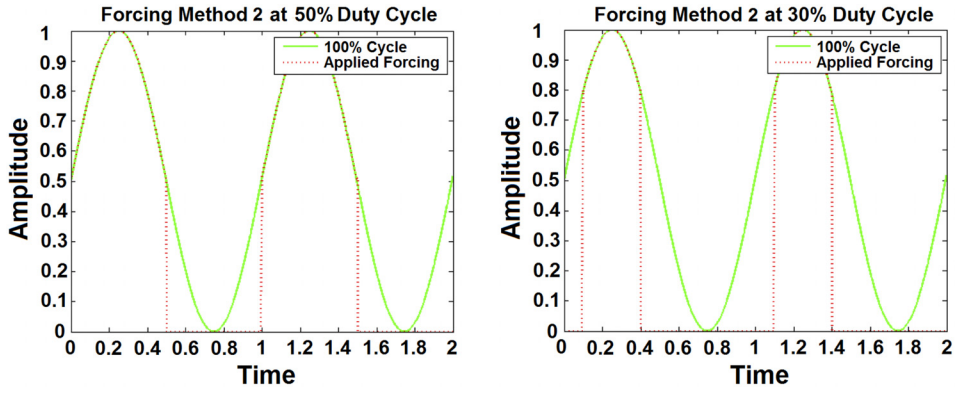

FIG. 3. Forcing profile 2 at duty cycle $\delta = 50\%$ (left) and $\delta = 30\%$ (right). This figure shows the more pulse like nature of the second Forcing profile, with the variable heater switched off in between pulses.

B. Experimental design and procedures

All experiments reported here were focused around a flow dominated by an azimuthal wavenumber 3 travelling baroclinic wave exhibiting a "modulated amplitude vacillation" (Read *et al.*, 1992). In this regime, the amplitude of the dominant wavenumber (its harmonics and, at least intermittently, its sidebands) was subject to a relatively fast, nearly periodic modulation (with a period of around 200 s) whose strength varied more slowly and cyclically (though aperiodically) on a timescale of around 1100 s. An example of a time series taken from an unperturbed experiment is shown in Fig. 4, which shows azimuth-time contour maps (or Hovmöller diagrams) of the variations of temperature at mid-radius and mid-height. The slow azimuthal drift of the wavenumber 3 pattern is apparent in the diagonal patterns of positive and negative temperature anomalies, while the fast oscillations of wave amplitude ("amplitude vacillations") are apparent in the break-up of the diagonal stripes into a braided or pulsating pattern. The depth of the modulation by the fast vacillation is seen to vary slowly in time, indicating that this is a "modulated amplitude vacillation regime." Modulations in the dominant wave amplitude were also accompanied by fluctuations in the advective heat transfer between the inner and outer sidewall (Read *et al.* 1992), which could also be affected by changes in ΔT, forming the basis for coupling the system to an oscillating heat source or sink (Castrejón-Pita *et al.*, 2010).

Intermittent synchronization experiments were typically initialized by setting the required mean temperature difference, ΔT_0, and rotation rate, Ω, and allowing the system to come to equilibrium, typically for 1–3 h. The modulation to ΔT was then applied with given values of ϵ, γ, and duty cycle δ held constant for intervals of at least 1 h (if synchronization was actually observed), or for up to 3 h if synchronization was not clearly evident. The value of γ was then incremented automatically in order to scan a range of frequencies, starting with a value at which permanent synchronization was not observed so that the onset of phase synchronization and subsequent phase-locking was clear. The experimental sequence was then repeated at a different duty cycle level (expressed as a percentage of each cycle) in order to map out where phase-locking was observed and then eventually lost, thereby delineating the "Arnol'd tongue" for that particular flow.

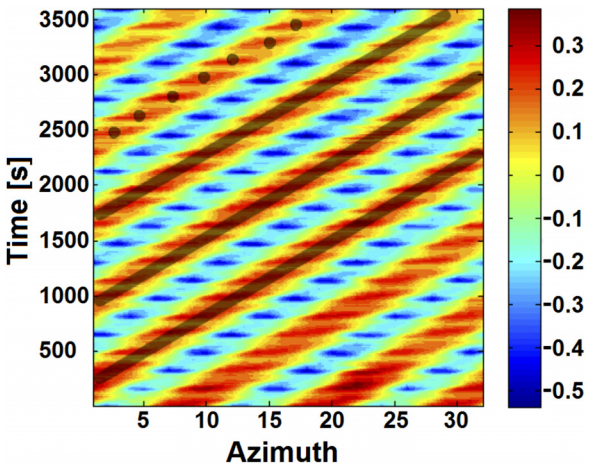

FIG. 4. Hovmöller (azimuth-time) diagram at mid-height and mid-radius of a 3 MAV flow. The contour colours show the amplitude of the temperature fluctuations around the mean in K. The dots detail the temperature vacillations and the lines indicate that it is a wave-3 regime drifting around the annulus with a period of approximately 2000 s.

C. Analysis procedures

During the whole experiment, temperature data and the rotation rate were logged for later analysis. Variations in the wave amplitude were determined from Fourier analyses in azimuth of the thermal measurements from the thermocouple ring at mid-height and mid-radius of the annulus at a given timestep. A fast Fourier transform of the 32 sensors in the ring at a given timestep enabled a decomposition of the thermal structure into azimuthal harmonics, from which the amplitudes and phases of the different components could be determined. An example is illustrated in Fig. 5, showing the complex spatio-temporal amplitude variations of wavenumbers 1, 2, and 3 which reveal the modulation of the dominant wave mode, its sideband, and long wave component, much as found by Read *et al.* (1992) and Früh and Read (1997).

In the same way as investigated by Eccles *et al.* (2009) and Castrejón-Pita *et al.* (2010), synchronization was sought between the applied periodic modulation of ΔT and the observed variation in amplitude of the dominant azimuthal wavenumber in temperature. This was determined from the

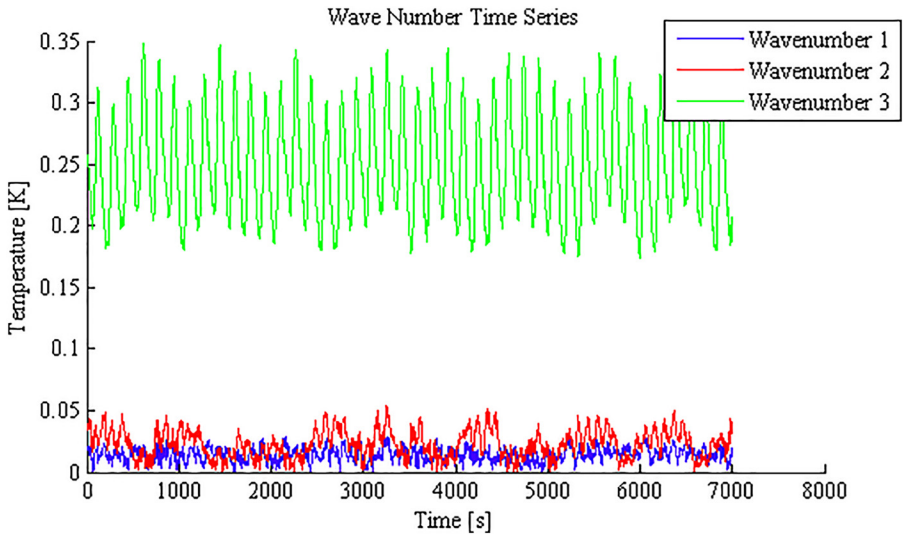

FIG. 5. Wavenumber amplitude time series, showing variations in the amplitudes of the azimuthal Fourier components of temperature for wavenumbers 1, 2, and 3. The dominant wavenumber is 3 and all three components clearly exhibit an oscillation where the amplitude is non-linear and varies over time.

time series of wave amplitude of the dominant wavenumber component. The phase of the amplitude oscillation was determined through analytical phase analysis via the Hilbert Transform method [e.g., as described by Pikovsky *et al.* (2001) and Boccaletti *et al.* (2002)]. This entailed construction of the complex timeseries

$$Y_m(t) = X_m(t) + iX_m^H(t), \tag{3}$$

where $X_m(t)$ is the measured timeseries of the amplitude of wavenumber m and $X_m^H(t)$ is its Hilbert Transform. The phase was then determined from

$$\varphi_m(t) = \tan^{-1}\frac{X_m^H(t)}{X_m(t)}. \tag{4}$$

$\varphi_m(t)$ is restricted by construction to the range $[0,2\pi]$, but accumulating the phases such that, following every cycle, $\varphi_m(t)$ increases or decreases by 2π (termed "unwrapping" of the phase), its increasing or decreasing value in time could be observed and compared with the phase of the forcing, given (without loss of generality) by

$$\varphi_F(t) = \gamma t. \tag{5}$$

Finally, by calculating the instantaneous phase difference,

$$\Delta\varphi(t) = \varphi_m(t) - \varphi_F(t), \tag{6}$$

phase synchronization signatures (typically related to near-stationary values of $\Delta\varphi$) could be identified and investigated. These included compiling histograms of $\Delta\varphi(\mathrm{mod}2\pi)$ and the synchronization index,

$$R = \left|\frac{1}{N}\sum_{k=1}^{N} e^{i\Delta\varphi(t_k)}\right|, \tag{7}$$

as a measure of phase coherence, where R takes the value of unity for perfect phase synchronization and zero for a uniform statistical distribution of phases (Mormann *et al.*, 2000). The observed frequencies or periods were also computed to study the frequency entrainment between forcing and response (e.g., Pikovsky *et al.*, 2001).

III. RESULTS

As described above, an unperturbed flow was set up at a nominal point in $(\Theta, \mathcal{T})$ parameter space at $(0.544, 6.81 \times 10^6)$, corresponding to a freely evolving wavenumber 3 MAV flow pattern which was weakly chaotic (e.g., Früh and Read, 1997). Upon application of full sinusoidal forcing of the boundary conditions at frequency γ with an amplitude $\varepsilon \approx 0.05\Delta T$, the vacillation phase was recorded and compared with the phase of the forcing to establish the extent to which it was phase-synchronized.

A. Duty cycle $\delta = 100\%$

Figure 6 shows some examples of phase difference timeseries $\Delta\varphi(t)$ and histograms of $\Delta\varphi(\mathrm{mod}2\pi)$ for three different forcing periods at the full 100% duty cycle that illustrate both fully synchronized [(c) and (d)] and partially synchronized [(a), (b), (e), and (f)] cases.

In cases where the detuning (difference between the forcing and natural vacillation periods) is too large for sustained, continuous synchronization, $\Delta\varphi(t)$ is seen either to increase [Fig. 6(a)] or decrease [Fig. 6(e)] monotonically with occasional phase slips, representing a partially synchronized state. In the fully synchronized case, however, [Fig. 6(c)] $\Delta\varphi(t)$ oscillates gently about a constant mean value. Even for the unsynchronized cases, however, the phase exhibits plateaux where $\Delta\varphi(t)$ appears to "pause" and remains nearly constant for a short while before resuming a drift. This is indicative of a nonlinear interaction between the forcing and vacillation in which the forcing partially affects the oscillation but not sufficiently to achieve a permanent synchronization, so is classified as a partial synchronization.

This is also evident in the histograms of $\Delta\varphi(\mathrm{mod}2\pi)$, which are not uniform across all phases, even for the unsynchronized cases shown in Fig. 6, also indicating a partially

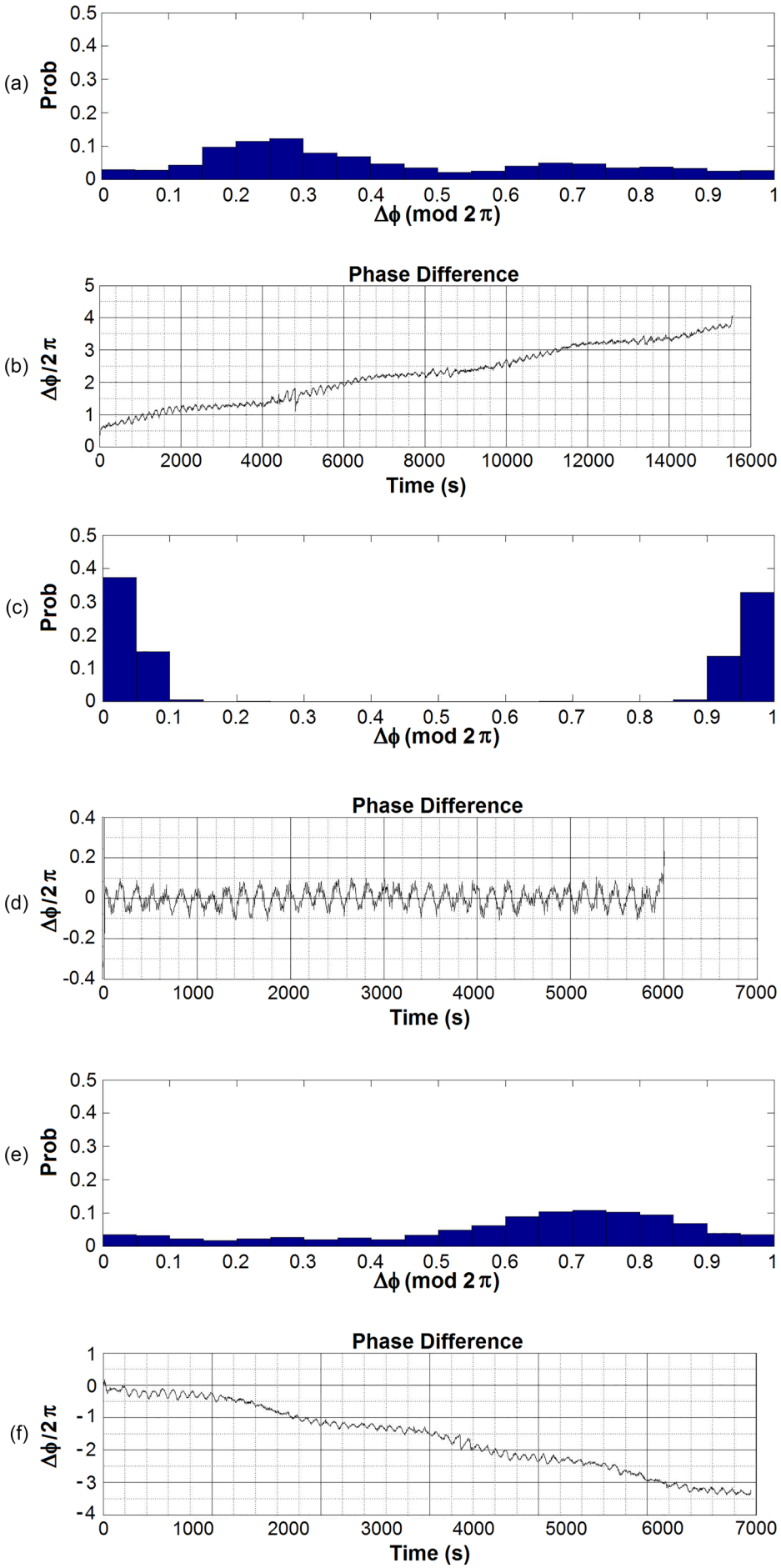

FIG. 6. Example timeseries of $\Delta\varphi(t)$ for wavenumber $m = 3$ with a duty cycle δ of 100%, showing variations at different forcing periods (τ_F) within and beyond the phase-locked region: (a) and (b) $\tau_F = 158$ s (partially synchronized), (c) and (d) $\tau_F = 166$ s (fully synchronized), and (e)-(f) $\tau_F = 174$ s (partially synchronized). Panels (b), (d), and (f) show the unwrapped timeseries of $\Delta\varphi(t)$ and (a), (c), and (e) show the corresponding histograms (mod 2π).

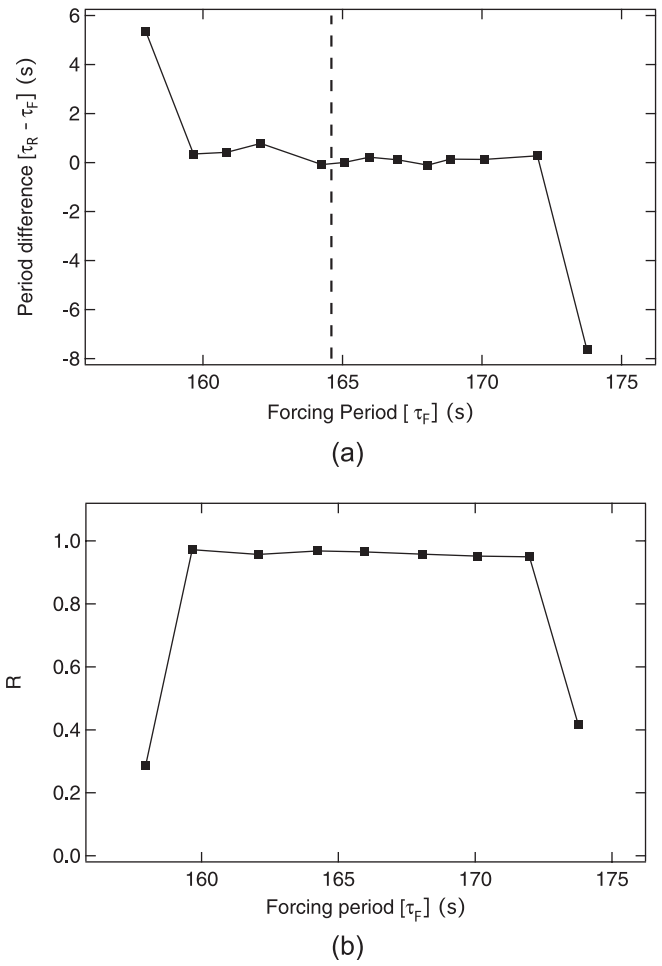

FIG. 7. Variation of (a) difference in period between wave amplitude vacillation and forcing, and (b) synchronization index, R, for wavenumber m = 3 with a duty cycle δ of 100%, as a function of forcing period τ_F. The dashed line in (a) indicates the mean natural period of the unperturbed vacillation.

synchronized state. The histogram for the fully synchronized state in Fig. 6(d) is sharply peaked, consistent with a roughly constant phase difference between forcing and response. For the other cases, however, all phases appear in the histograms in Figs. 6(b) and 6(f) but with peaks at certain favoured values of $\Delta\varphi$. This indicates some degree of partial synchronization.

Other measures of the degree of synchronization for these cases are illustrated in Fig. 7, showing (a) the mean difference in the oscillation period between observed vacillation and the forcing, and (b) the synchronization index, R [cf. Eq. (7)] over a range of forcing periods, τ_F, from ∼158 s to 174 s. Figure 7(a) clearly shows a plateau in $\Delta\tau = \tau_R - \tau_F$ from $\tau_F = 160$ s to 172 s around a natural vacillation period of approximately 164.5 s, with a markedly different τ_R outside this range, more or less consistent with the difference in period between τ_F and the natural period. The loss of synchronization outside this interval is also clearly seen in the profile of R in Fig. 7(b), which takes values close to 1 within the synchronized interval and exhibits a sharp drop-off towards smaller values beyond it. The value of R at $\tau_F = 158$ s and 174 s, however, does not drop immediately to zero but remains finite, indicative of partial but incomplete phase synchronization in which the monotonic progression of $\Delta\varphi(t)$ with time pauses temporarily in metastable synchronized states, followed by more rapid phase slips as synchronization is lost [e.g., see Figs. 6(b) and 6(f)].

B. Other duty cycles

Other duty cycles were investigated for both forcing profiles in sequences in which the forcing period was incremented successively over the same range as for the 100% duty cycle. The vacillation response was recorded as above for intervals of 1–3 h before incrementing the forcing period to the next value. The experiment was typically run continuously without stopping throughout each sequence at a given duty cycle and forcing profile.

The degree of synchronization was determined as for the 100% duty cycle presented in Sec. III A and Fig. 8 illustrates the complete results in terms of the period difference $\Delta\tau$ for (a) forcing profile 1 and (b) forcing profile 2. For both forcing profiles, the interval in τ_F over which frequency entrainment and synchronization occur is seen to be a strong function of duty cycle, with the interval decreasing towards zero as the duty cycle was reduced. The boundary of the synchronized region is shown with bold lines in Fig. 8, showing

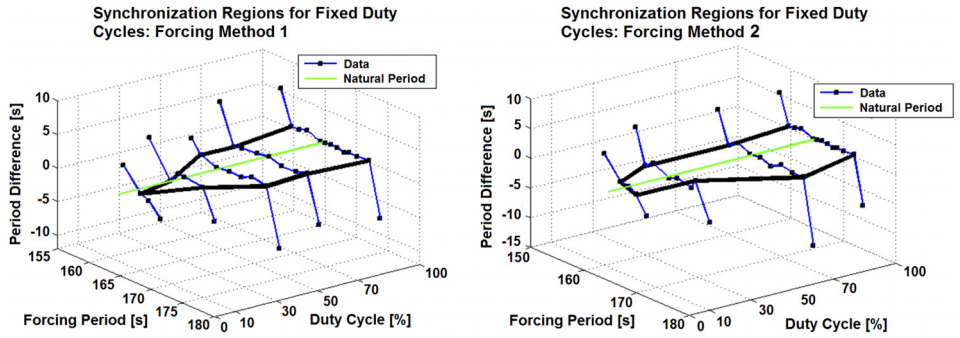

FIG. 8. 3D plot of the period difference between forcing and response for fixed duty cycles using forcing profile 1 (left) and forcing profile 2 (right). These graphs show the boundaries of the phase synchronized regions (Arnol'd Tongues) as heavy black lines in each case. The results for forcing profile 2 show that the system became identifiably synchronized with a duty cycle as low as 10%, although a similar degree of synchronization required a duty cycle of ∼30% for forcing profile 1.

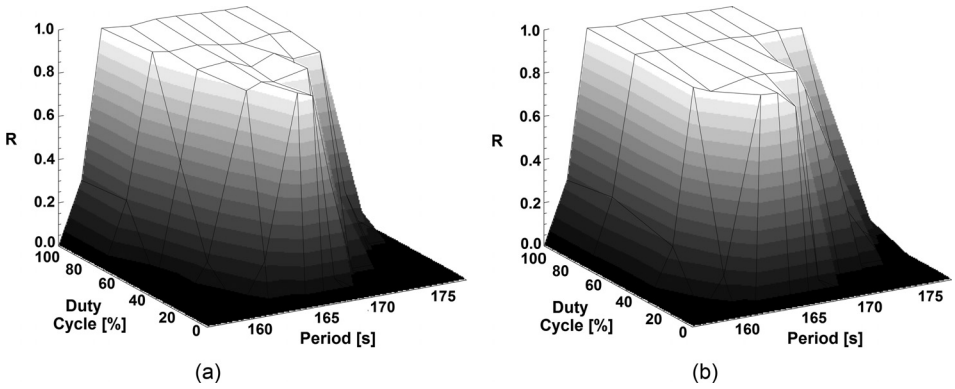

FIG. 9. 3D plot of the synchronization index for fixed duty cycles and variable forcing period using Forcing profile 1 (left) and Forcing profile 2 (right). These graphs show the Arnol'd Tongues (black lines) of the system depending on the Forcing profile. The results for Forcing profile 2 show that the system synchronized with a duty cycle as low as 10%, showing that there are some small differences in the width of the region of synchronization depending on the Forcing profile.

the convergence of the boundaries as δ is decreased. This was more pronounced for forcing profile 1, however, for which the synchronization interval was found to shrink to almost zero by $\delta = 10\%$. For forcing profile 2, however, a significant interval of synchronization was evident even at $\delta = 10\%$. In fact, for forcing profile 2, the synchronized interval in τ_F at $\delta = 70\%$ actually seemed to increase slightly over the value at $\delta = 100\%$, although this may be only a marginal effect. The corresponding variations of R for these two forcing profiles as a function of duty cycle δ are shown in Fig. 9, for comparison with Fig. 8. These both show a plateau in R close to $R = 1$, indicating complete phase synchronization, with steep sides that demonstrate the rapid loss of synchronization as the detuning in τ_F becomes too large. The sides are not completely vertical, however, indicating that some weak partial synchronization is retained even outside the Arnol'd tongue, although this decays rapidly as the detuning becomes larger. As with the profiles of $\Delta\tau$, the width of the plateaux becomes steadily narrower as δ is reduced, but with a greater effect notable for forcing profile 1 compared with forcing profile 2.

Some typical timeseries of the wave amplitude and $\Delta\varphi(t)$ (normalized by 2π) are illustrated in Fig. 10 for a range of duty cycle δ from 10% to 100% using forcing profile 2 with a forcing period of $\tau_F = 162$ s. Together with Fig. 6(d), this clearly shows that, even when fully synchronized, $\Delta\varphi(t)$ oscillates about its mean value at a period of τ_F, though does not drift. The amplitude modulation index and intensity of the irregular fluctuations of the spatial sidebands are relatively unaffected by phase-synchronizing with the periodic forcing, with sporadic fluctuations in the modulation index of $m = 3$ even at large values of δ. The azimuthal propagation of the baroclinic waves (not shown) is also not much affected by the synchronization, which is largely confined to entraining the phase of the main oscillation in wave amplitude and associated variations in heat transfer.

As δ is reduced, however, the amplitude of phase fluctuations is seen to increase, especially at the lowest values of δ. This is clearly shown in Table II, which shows the standard deviation of phase difference fluctuations $\sigma_{\Delta\varphi}$ (normalized by 2π) as a function of δ for two values of τ_F within the fully synchronized region, where the subscript number indicates the forcing profile. Even though the flow remains synchronized down to the smallest values of δ in both cases, the amplitude of the oscillations in $\Delta\varphi(t)$ nearly doubles in size from their value at $\delta = 100\%$ by $\delta = 10\%$, roughly consistent with a scaling that follows the form

$$\sigma_{\Delta\varphi} \sim \sigma_0 \delta^{-\mu}, \tag{8}$$

where $\sigma_0 (= 0.0399 \pm 0.0013)$ is the value of $\sigma_{\Delta\varphi}$ at $\delta = 100\%$ and μ is an exponent with a fitted value around $\mu = 0.247 \pm 0.027$ for forcing profile 1 at $\tau_F = 164$ s. The data for both forcing profiles and the corresponding fit to profile 1 are shown in Fig. 11.

IV. DISCUSSION

In this paper, we have extended the experiments of Eccles *et al.* (2009) to demonstrate that a high degree of phase synchronization occurs between oscillations in baroclinic wave amplitude and imposed variations in boundary temperatures, even when these variations are only imposed for a fraction of the oscillation cycle as small as 10%. This, and the observation of similar degrees of synchronization for two quite different forcing profiles, clearly illustrates the robustness of this synchronization phenomenon, depending only on the coherence and repeatability of the forcing signal and not its precise waveform. The systematic variation in the width of the synchronized region in τ_F defines a wedge-shaped region resembling an Arnol'd tongue, indicating that the duty cycle parameter δ plays a similar role to a coupling coefficient in a more conventional, steadily forced, master-slave pair of coupled oscillators.

Immediately outside the fully phase-synchronized region, the oscillations in wave amplitude are only partially synchronized but still exhibit noticeable temporary plateaux in $\Delta\varphi(t)$, indicating that the periodic forcing is still exerting an influence on the amplitude oscillations, though not sufficient to constrain $\Delta\varphi(t)$ to a quasi-stationary value. The interval between such phase plateaux evidently increases as the detuning in τ_F increases. This time interval would be expected to exhibit scaling behavior as the boundary of the Arnol'd tongue is approached (e.g., Boccalletti *et al.*, 2002), but many more experiments than were possible in the present study would be needed to confirm this.

Some indicative evidence for scaling in the amplitude of fluctuations in $\Delta\varphi(t)$ within the Arnol'd tongue itself was found, however, which appears to exhibit a deterministic periodic component as well as stochastic noise. This would

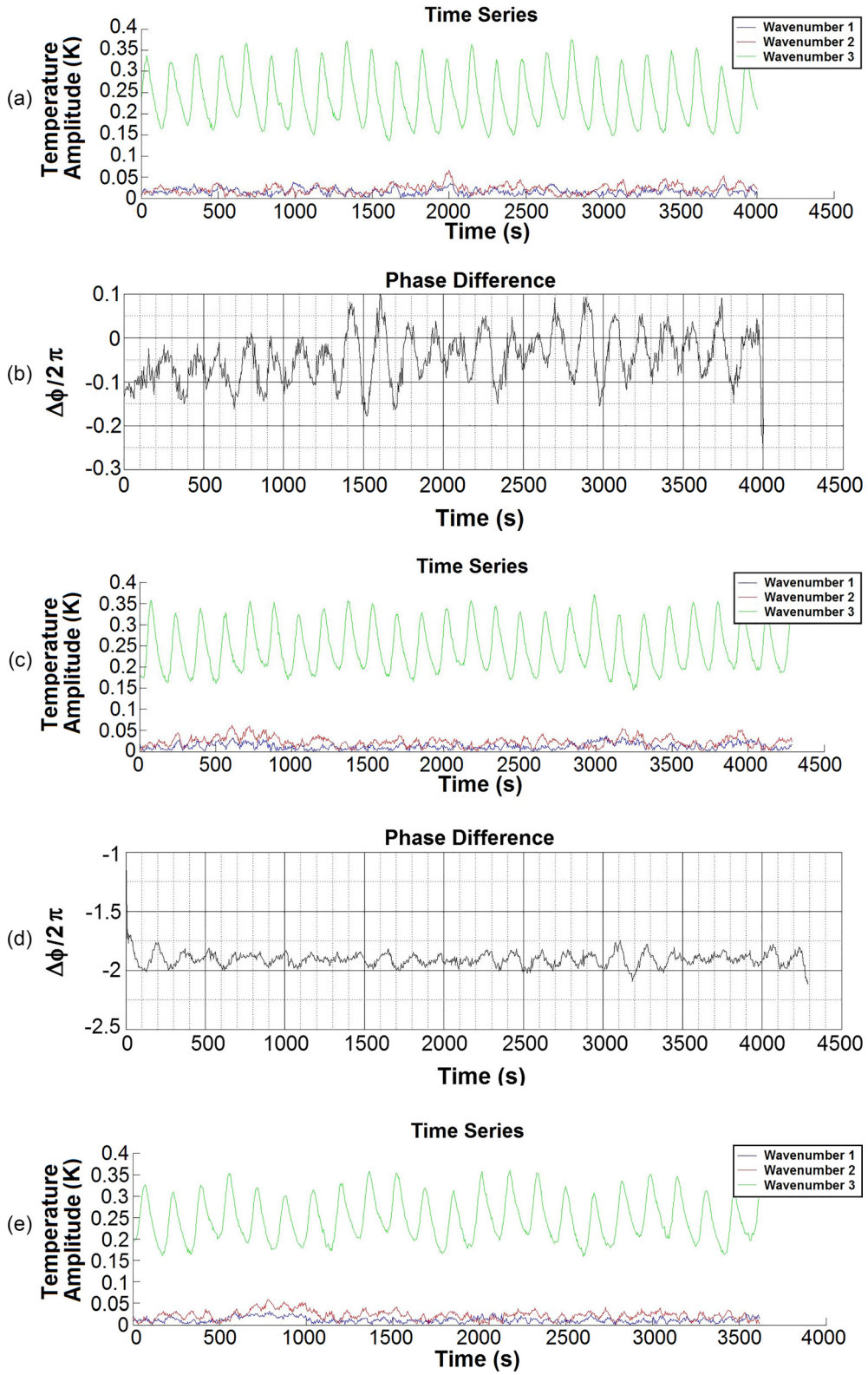

FIG. 10. Time series of wave amplitude [(a), (c), (e), and (g)] and $\Delta\varphi(t)/2\pi$ [(b), (d), (f), and (h)] for forcing profile 2 at a period of 162 s and duty cycles of 100% [(a) and (b)], 70% [(c) and (d)], 30% [(e) and (f)], and 10% [(g) and (h)]. Note the change in the vertical and horizontal scales across panels.

suggest the effects of a higher order nonlinearity in the phase dynamics than is typically assumed (e.g., Boccalletti *et al.*, 2002). The data are roughly consistent with a power law dependence which could suggest a growth of the variance of these fluctuations as $\delta^{-1/2}$ which deserves further attention in future theoretical work, especially if such behavior was common to other phase-synchronized systems. It would be of significant interest to explore other aspects of scaling related to this kind of phase synchronization in the laboratory, although the long duration of experiments needed to

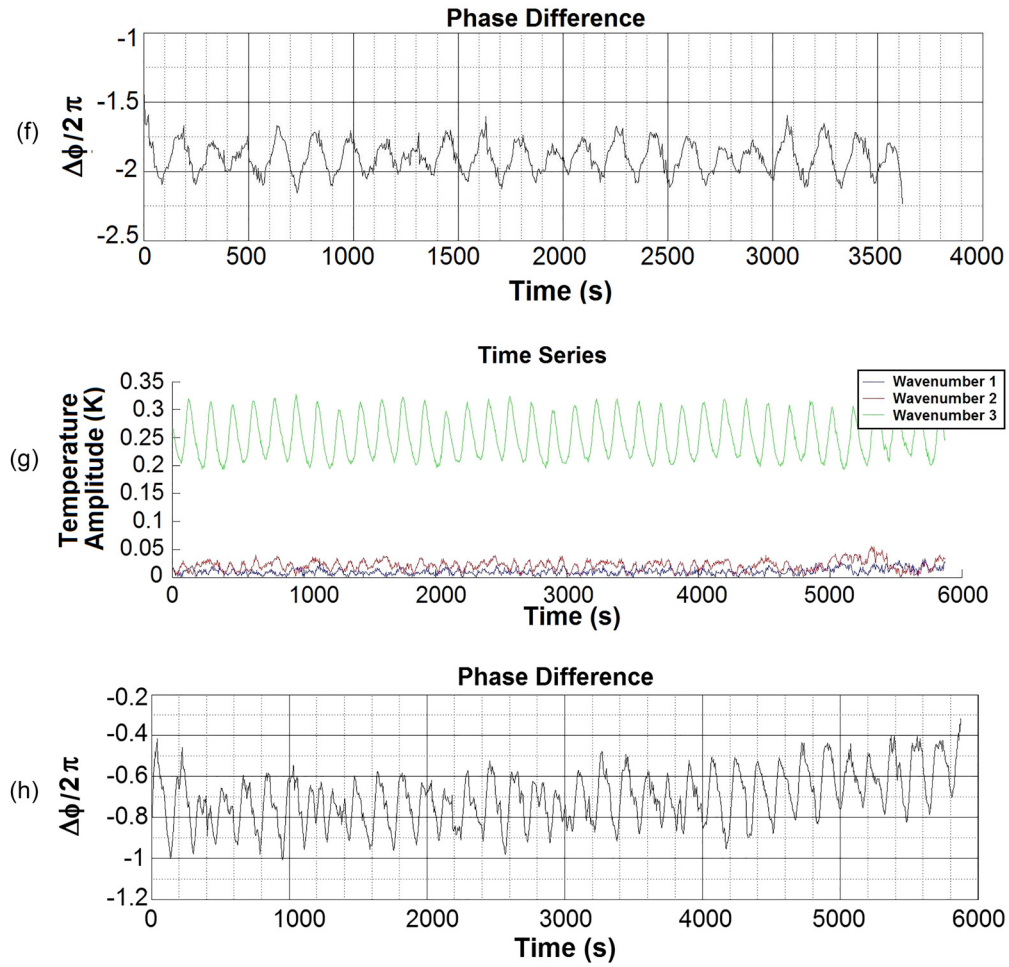

FIG. 10. (*Continued.*)

acquire sufficient statistics to identify and characterize such scaling relationships represents a formidable task.

As mentioned above, a significant motivation for the present study was a possible analogy between these experiments and models of synchronized teleconnections in the climate system of the Earth and other planets. Recent explanations for observed teleconnections have tended to focus on mechanisms involving the propagation of information across the planet via trains of planetary Rossby waves, which may be launched from anomalies of surface heating or topography (Hoskins and Karoly, 1981). This would tend to imply coupling via non-axisymmetric eddies in model simulations exploring synchronized teleconnections (cf. Duane *et al.*, 1999; Lunkheit, 2001; and Duane and Tribbia, 2001). In the present case, however, and in the earlier work of Eccles *et al.* (2009) and Castrejón-Pita and Read (2010), coupling was implemented via the axisymmetric boundary conditions, effectively coupling the zonally symmetric "annular modes," leaving the waves and eddies within the system to determine a secondary response to this type of forcing. The results presented here and by Eccles *et al.* (2009) and Castrejón-Pita and Read (2010) show that such annular mode forcing can also lead to a more subtle form of synchronized teleconnection that directly affects only the zonally symmetric flow though may influence the overall amplitude of wave activity indirectly. This kind of teleconnection could well play a role in the dynamics of annular modes in the climate system, such as the North Atlantic and Arctic Oscillations (Hurrell *et al.*, 2003).

The present work, moreover, indicates that even if such annular coupling were to be significantly modulated (or even interrupted intermittently), e.g., by circulation changes during the seasonal cycle, such that it might actually decouple remote regions for significant fractions of the year, this would not preclude the possibility of significant coherent interactions that would appear as correlated cyclic behaviours between climatic components in different parts of the globe. Such a propensity for teleconnected synchronization may have significant implications, e.g., for seasonal forecasting of the climate or on longer timescales and should be explored further using more detailed and realistic models.

TABLE II. Standard deviation of $\Delta\varphi(t)/2\pi$ as a function of δ.

Duty cycle δ (%)	$\sigma_{\Delta\varphi 1}$ ($\tau_F = 164$ s) rad/2π	$\sigma_{\Delta\varphi 2}$ ($\tau_F = 162$ s) rad/2π
100	0.041	0.048
70	0.043	0.046
50	0.045	
30	0.057	0.056
10	0.070	0.071

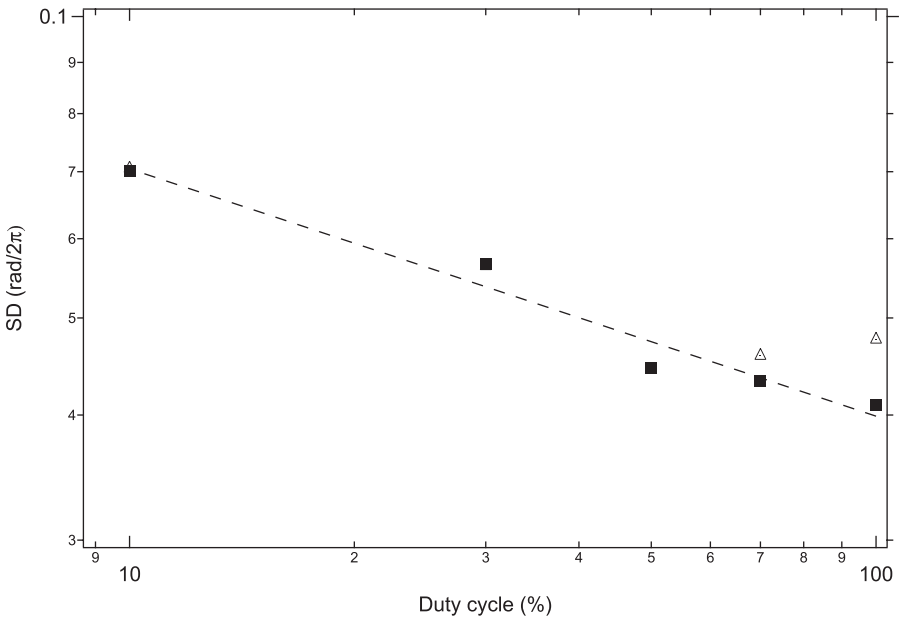

FIG. 11. Variation of the amplitude of fluctuations in phase difference [measured by the standard deviation of $\Delta\varphi(t)$] with duty cycle δ for forcing profile 1 (at $\tau_F = 164\,\mathrm{s}$) and forcing profile 2 (at $\tau_F = 162\,\mathrm{s}$). The fit of the scaling function in Eq. (8) to $\sigma_{\Delta\varphi 1}$ is shown as a dashed line in this log-log plot. Filled squares represent data using forcing profile 1 and open triangle profile 2.

ACKNOWLEDGMENTS

P.L.R., A.A.C.P., and X.M.-A. acknowledge the U.K. Natural Environment Research Council for its support of the early stages of this work, under Grant Reference No. NE/F002157/1 and a Research Experience Internship, respectively. Thanks are also due to Dr. Sam Marshall for assistance and advice during the experiments. A.A.C.P. was also supported by the Royal Society.

Abarbanel, H. D. I., Creveling, D. R., Farsian, R., and Kostuk, M., "Dynamical state and parameter estimation," SIAM J. Appl. Dyn. Syst. **8**(4), 1341–1381 (2009).

Arenas, A., Díaz-Guilera, A., Kurths, J., Moreno, Y., and Zhou, C., "Synchronization in complex networks," Phys. Rep. **469**, 93–153 (2008).

Boccaletti, S., Kurths, J., Osipov, G., Valladares, D., and Zhou, C., "The synchronization of chaotic systems," Phys. Rep. **366**, 1–101 (2002).

Castrejón-Pita, A. A. and Read, P. L., "Synchronization in a pair of thermally coupled rotating baroclinic annuli: Understanding atmospheric teleconnections in the laboratory," Phys. Rev. Lett. **104**, 204501 (2010).

Cheng, N. S., *Formula for Viscosity of Glycerol-Water Mixture* (School of Civil and Environmental Engineering, Nanyang Technological University, Singapore, 2008).

Cristancho, D., Delgado, D., Martínez, F., Abolghassemi Fakhree, M., and Jouyban, A., "Volumetric properties of glycerol + water," Rev. Colomb. Cienc. Quím. Farm. **40**(1), 92–115 (2011).

Duane, G., "Synchronized chaos in extended systems and meteorological teleconnections," Phys. Rev. E **56**, 6475 (1997).

Duane, G. S., "Synchronicity from synchronized chaos," Entropy **17**(4), 1701–1733 (2015).

Duane, G. S. and Tribbia, J. J., "Synchronized chaos in geophysical fluid dynamics," Phys. Rev. Lett. **86**(19), 4298–4301 (2001).

Duane, G. S. and Tribbia, J. J., "Weak Atlantic-Pacific teleconnections as synchronized chaos," J. Atmos. Sci. **61**(17), 2149–2168 (2004).

Duane, G. S., Tribbia, J. J., and Weiss, J. B., "Synchronicity in predictive modelling: A new view of data assimilation," Nonlinear Proc. Geophys. **13**(6), 601–612 (2006).

Duane, G. S., Webster, P. J., and Weiss, J. B., "Co-occurrence of northern and southern hemisphere blocks as partially synchronized chaos," J. Atmos. Sci. **56**, 4183–4205 (1999).

Eccles, F. J., Read, P. L., Castrejón-Pita, A. A., and Haine, T. W., "Synchronization of modulated traveling baroclinic waves in a periodically forced, rotating fluid annulus," Phys. Rev. E **79**, 015202(R) (2009).

Feliks, Y., Ghil, M., and Robertson, A. W., "Oscillatory climate modes in the eastern mediterranean and their synchronization with the north atlantic oscillation," J. Clim. **23**, 4060–4079 (2010).

Fowlis, W. W. and Hide, R., "Thermal convection in a rotating annulus of liquid: Effect of viscosity on the transition between axisymmetric and non-axisymmetric flow regimes," J. Atmos. Sci. **22**, 541–558 (1965).

Früh, W.-G. and Read, P. L., "Wave interactions and the transition to chaos of baroclinic waves in a thermally driven rotating annulus," Philos. Trans. R. Soc. London **355**, 101–153 (1997).

Glass, L., "Synchronization and rhythmic processes in physiology," Nature **410**, 277–284 (2001).

Goldstein, R. E., Lauga, E., Pesci, A. I., and Proctor, M. R. E., "Elastohydrodynamic synchronization of adjacent beating flagella," Phys. Rev. Fluids **1**, 073201 (2016).

Gruzdev, A. N. and Bezverkhny, V. A., "Two regimes of the quasi-biennial oscillation in the equatorial stratospheric wind," J. Geophys. Res. **105**, 29435–29443, doi:10.1029/2000JD900495 (2000).

Hide, R. and Mason, P. J., "Sloping convection in a rotating fluid," Adv. Phys. **24**, 47–100 (1975).

Hiemstra, P. H., Fujiwara, N., Selten, F. M., and Kurths, J., "Complete synchronization of chaotic atmospheric models by connecting only a subset of state space," Nonlinear Proc. Geophys. **19**(6), 611–621 (2012).

Hignett, B. P., White, A. A., Carter, R. D., Jackson, W. D., and Small, R. M., "A comparison of laboratory measurements and numerical simulations of baroclinic wave flows in a rotating cylindrical annulus," Q. J. R. Meteorol. Soc. **111**, 131–154 (1985).

Hoskins, B. J. and Karoly, D., "The steady linear response of a spherical atmosphere to thermal and orographic forcing," J. Atmos. Sci. **38**, 1179–1196 (1981).

Hurrell, J. W., Kushnir, Y., Ottersen, G., and Visbeck, M. (eds.), *The North Atlantic Oscillation: Climatic Significance and Environmental Impact* (American Geophysical Union, Washington, DC, 2003).

Kocarev, L., Tasev, Z., and Parlitz, U., "Synchronizing spatiotemporal chaos of partial differential equations," Phys. Rev. Lett. **79**, 51–54 (1997).

Kuai, L., Shia, R. L., Jiang, X., Tung, K. K., and Yung, Y. L., "Nonstationary synchronization of equatorial QBO with SAO in observations and a model," J. Atmos. Sci. **66**, 1654–1664 (2009).

Lorenz, E. N., "Dimension of weather and climate attractors," Nature **353**, 241–244 (1991).

Lunkeit, F., "Synchronization experiments with an atmospheric global circulation model," Chaos **11**, 47–51 (2001).

Maestrello, L., "Synchronized turbulent boundary layer-flexible structure by sound and transient shock wave," AIAA J. **42**, 920–930 (2004).

Maraun, D. and Kurths, J., "Epochs of phase coherence between El Niño/Southern oscillation and Indian monsoon," Geophys. Res. Lett. **32**, L15709, doi:10.1029/2005GL023225 (2005).

Maza, D., Vallone, A., Mancini, H., and Boccaletti, S., "Experimental phase synchronization of a chaotic convective flow," Phys. Rev. Lett. **85**, 5567–5570 (2000).

Mormann, F., Lehnertz, K., David, P., and Elger, C. E., "Mean phase coherence as a measure for phase synchronization and its application to the EEG of epilepsy patients," Physica D **144**, 358–369 (2000).

Pecora, L. M., Carroll, T. L., Johnson, G. A., Mar, D. J., and Heagy, J. F., "Fundamentals of synchronization in chaotic systems, concepts, and applications," Chaos **7**, 520–543 (1997).

Pikovsky, A., Rosenblum, M., and Kurths, J., *Synchronization: A Universal Concept in Nonlinear Sciences* (Cambridge University Press, New York, 2001).

Pereira, F. A. C., Colli, E., and Sartorelli, J. C., "Synchronization of two bubble trains in a viscous fluid: Experiment and numerical simulations," Phys. Rev. E **87**, 022917 (2013).

Read, P. L., "A combined laboratory and numerical study of heat transport by baroclinic eddies and axisymmetric flows," J. Fluid Mech. **489**, 301–323 (2003).

Read, P. L., Bell, M. J., Johnson, D. W., and Small, R. M., "Quasi-periodic and chaotic flow regimes in a thermally driven, rotating fluid annulus," J. Fluid Mech. **238**, 599–632 (1992).

Read, P. L. and Castrejón-Pita, A. A., "Synchronization in climate dynamics and other extended systems," in *Nonlinear Dynamics and Chaos: Advances and Perspectives, Understanding Complex Systems*, edited by M. Thiel, J. Kurths, M. C. Romano, A. Moura, and G. Károlyi (Springer-Verlag, 2010), pp. 153–176.

Read, P. L. and Castrejón-Pita, A. A., "Phase synchronization between stratospheric and tropospheric quasi-biennial and semi-annual oscillations," Q. J. R. Meteorol. Soc. **138**, 1338–1349 (2012).

Read, P. L., Pérez, E. P., Moroz, I. M., and Young, R. M. B., "General circulation of planetary atmospheres: Insights from rotating annulus and related experiments," in *Modeling Atmospheric and Oceanic Flows: Insights from Laboratory Experiments and Numerical Simulations*, edited by T. von Larcher and P. D. Williams (AGU and Wiley, New Jersey, USA, 2015), pp. 9–44.

Rosenblum, M. G., Pikovsky, A. S., and Kurths, J., "Phase synchronization of chaotic oscillators," Phys. Rev. Lett. **76**, 1804–1807 (1996).

Rulkov, N. F., Sushchik, M. M., and Tsimring, L. S., "Generalized synchronization of chaos in directionally coupled chaotic systems," Phys. Rev. E **51**, 980–994 (1995).

Shen, M.-L., Keenlyside, N., Selten, F., Wiegerinck, W., and Duane, G. S., "Dynamically combining climate models to "supermodel" the tropical Pacific," Geophys. Res. Lett. **43**, 359–366, doi:10.1002/2015GL066562 (2016).

Stein, K., Timmermann, A., and Schneider, N., "Phase synchronization of the El-Niño Southern oscillation with the annual cycle," Phys. Rev. Lett. **107**, 128501 (2011).

Taylor, A. F., Tinsley, M. R., Wang, F., Huang, Z., and Showalter, K., "Dynamical quorum sensing and synchronization in large populations of chemical oscillators," Science **323**(5914), 614–617 (2009).

van den Berge, L. A., Selten, F. M., Wiegerinck, W., and Duane, G. S., "A multi-model ensemble method that combines imperfect models through learning," Earth Syst. Dyn. **2**(1), 161–177 (2011).

Van Wiggeren, G. D. and Roy, R., "Communication with chaotic lasers," Science **279**(5354), 1198–1200 (1998).

Watts, D. J. and Strogatz, S. H., "Collective dynamics of 'small-world' networks," Nature **393**, 440–442 (1998).

Williamson, C. H. K. and Govardhan, R., "Vortex-induced vibrations," Ann. Rev. Fluid Mech. **36**, 413–455 (2004).

Yang, S.-C., Baker, D., Li, H., Cordes, K., Huff, M., Nagpal, G., Okereke, E., Villafañe, J., Kalnay, E., and Duane, G. S., "Data assimilation as synchronization of truth and model: Experiments with the three-variable Lorenz system," J. Atmos. Sci. **63**(9), 2340–2354 (2006).